Aerodynamic tunnel for tests of turbine annular cascades

Alexandr Lapuzin[1], Valery Subotovich[1], Yuriy Yudin[1] and Ivan Malymon[1*]

*Correspondence:
sevcrimea13@gmail.com

[1] National Technical University "Kharkiv Polytechnic Institute", Kharkiv 61002, Ukraine

Abstract

Aerodynamic test rigs are necessary for experimental testing of turbomachines and investigation of possible ways to improve machine performance. Existing installations give higher losses and do not work efficiently at off-design operating modes. An operating part with an adjustable radial diffuser was designed in order to determine the characteristics of turbine annular cascades. Experimental studies and computational verifications showed satisfactory results at various operating modes. The regulated backwall of the radial diffuser ensured supersonic velocity values behind the cascade and overall stable operation in a wide range of Mach numbers up to 1.3 when using compressors of comparatively small capacity. The optimum positions of the regulated backwall were determined, which provided a deep vacuum behind the cascade, as well as 1.5 times Mach number increase compared to the turbine cascade without a diffuser. Changing the inlet channel geometry at supersonic modes leads to an increase in the diffuser efficiency. Additionally, it was determined that the use of the turbine vane cascade in the test rig flow path is not necessary during calculation studies, but instead an axisymmetric vaneless converging area can be applied and give satisfactory results as well as reduce the time spent on calculations. The computational model can be used to optimize the design of an aerodynamic tunnel outlet area.

Keywords: Aerodynamic tunnel, Turbine annular cascade, Mach number, Radial diffuser, Swirled flow, Axisymmetric vaneless area

1 Introduction

Aerodynamic tunnels for tests of turbine annular cascades are divided into three categories depending on their operating time [1]: 1) Continuous type – operation during several hours in an open or a closed circuit; 2) Blowdown type – expulsion or suction lies between several seconds and several minutes; 3) Transitional operation – less than two seconds with an exhaust to the vacuum tank.

  Tunnels of transitional operation (the 3rd category) are a subcategory of blowdown operation tunnels; however, their very short operation time places them to a separate class according to the measuring technology type. Mostly, the same measuring devices are applied to the tunnels of the 1st and the 2nd categories, except for the

hot tests. The following aspects should be taken into consideration when choosing the tunnel type for the tests: the desired level of flow simulation – its high and low velocities, the need to change the Reynolds number, the temperature simulation in the case of cooling turbine blades, the size of the blades, etc.; the financial resources; the measurement and data collection methods that will be applied to the object.

Many tests within turbine cascades at a supersonic velocity are executed in the tunnels of blowdown operation: for instance, the aerodynamics tunnel in Virginia [2–9], a high-speed wind tunnel in Carleton University, Canada [10–13]. The experiment time depends on the size of the cascade's throat area and usually takes 20–60 s. Air humidity and condensed water steam are the disadvantages of blowdown operation tunnels. These factors substantially destroy the uniformity of the flow in the operating part of the aerodynamic tunnel and require aerodynamic tunnel complication because dehumidifiers and air heaters are needed. Tunnels of continuous operation with an open circuit are the most preferable as per turbine cascades' return on research [1].

The compressor engine power N, which forces the air, plays a big role when investigating turbine cascades, especially in aerodynamic tunnels of continuous operation at transonic modes. The analysis of the influence of main parameters demonstrates that the engine power is in direct ratio to the Mach number at the cascade outlet, to the square of the Reynolds number and to the cube of the temperature, while it is in inverse ratio to the pressure in the operating part and to the aerodynamic quality factor of the installation (rig). The proportionality of the power N to the square of the Reynolds number does not enable to maintain the simulation on this parameter in the majority of cases. It is advisable to experiment with a less than full-scale Reynolds number when investigating the turbine cascades with high Mach numbers and low dependence of the characteristics on the Reynolds number, which allows decreasing the compressor drive power substantially. It's also appropriate to take the following steps in order to decrease the compressor drive power: to increase the pressure, to reduce the temperature to a certain degree (since this can cause icing of the operating part and of the aerodynamic probes), to increase the aerodynamic quality factor of the installation, which can be increased up to 3 if a good diffuser behind the operating part is available [14].

To understand the processes which happen within real turbines, three models are usually used: stationary linear (flat) cascades (the 1st model), annular cascades (the 2nd model), and more complicated annular rotating cascades (the 3rd model). Experiments with the 3rd model are much more expensive and require more time to prepare and to perform an experiment. Installations that investigate linear cascades allow solving a big variety of tasks at moderate power of a compressor drive. The preparation and execution of such an experiment is much easier than those with annular cascades: a smaller number of blades is required to test linear cascades (linear cascades usually contain 5 to 10 blades); it is easier to measure the flow entry angles, and the air consumption per installation is lower as well. When testing transonic and supersonic linear cascades in aerodynamic tunnels at moderate compressor power, a flat diffuser with adjustable walls is installed behind the cascade, which requires an increase in the axial dimension of the installation to recover pressure efficiently [1, 14–16]. Some experiments that use a less powerful compressor are performed with a minimum number of blades [17], applying

convex and concave blade sides to the model boundaries. In such cases, one or two channels are tested (one whole blade inside). It is worth noting that reducing the number of blades leads to experimental error increase and to operating part complication due to the necessity of boundary layer suction.

The general disadvantage of linear cascade experiments is the inability to model radial gradient parameters behind the turbine cascade, as well as different cascade steps at the hub and at the periphery, which is essential when investigating cascades with a small ratio of average diameter to blade length.

Annular cascades are closer to real conditions. The flow at the turbine cascades' outlet is usually highly twisted. Correct boundary conditions behind the cascade must be ensured in the aerodynamic tunnels. Four options of output boundary conditions are known for linear cascades with highly twisted flow [18–26]. In the first and the easiest case, an annular channel with a constant hub and tip radius is installed behind the cascade, including the possibility of a transition to a sudden expansion channel [18–21]. However, if the flow is too twisted at the very beginning of the annular section, the flow might separate from the hub. The separated flow is not stationary and influences the radial pressure gradient that is reflected in the cascade characteristics.

In the second case, perforated devices are installed at the cascade outlet to imitate the operating cascade [22, 23]. Spurr [22] described a method of establishing the correct flow distribution at the cascade outlet with a low pressure gradient. Perforated plates with radial change of perforation were installed to imitate an impeller of the steam turbine last stage. Squire [23] applied the same technique at the outlet of the turbine's transonic cascade. In many cases, the authors consider that the use of a rotor to model the pressure gradient at the linear cascade's outlet is unnecessary. However, the additional resistance at the cascade's outlet reduces the aerodynamic tunnel capacity to obtain high-speed flow, especially at transonic modes, because the resistance of the perforated plate increases in direct ratio to the square of the velocity that requires higher power of the compressor drive.

In the third case, an unwinding cascade, which gave an axial direction to the flow, was installed downstream. Povey et al. [24] installed a stationary impulse rotor cascade, which was cut at mid-section, behind the tested cascade in the aerodynamic tunnel of the University of Oxford, which functioned as a deswirl system. The tests were performed both with full circuit air supply and in saving mode with a reduced number of blades within the sector model, similar to a flat cascade. Despite the compact design, the impulse operating cascade does influence the upstream flow and adds additional resistance at the outlet, which limits the possibility to obtain high flow velocity behind the tested cascade at the given compressor power.

In the fourth case, a diffuser was installed behind the annular cascade [25, 26]. In this case, the form of the diffuser is of particular importance due to the high flow swirl behind the turbine cascade and the high velocity level. Donovan [25] used an annular conical diffuser behind the nozzle grid. However, our tests proved that such diffusers do not ensure good pressure recovery at high flow swirls. The scientists at the Whittle Laboratory [26] used an axial-radial diffuser in the annular cascade, within which the circumferential velocity component decreases due to an increase of the flow path's radius that improves the diffuser characteristics, decreases the pressure, and increases

the Mach number behind the cascade compared to the annular conical diffuser. At the same time, the diffuser with a stationary position of contours and a relatively large length of axial diffuser has an increased hydraulic resistance and a high probability of diffuser "chocking" at relatively low flow velocity. At the same time, further increase of the flow velocity behind the cascade to obtain its characteristics in a wider range of Mach numbers becomes impossible even with a significant increase of drive power.

The literature review on aerodynamic tube designs for investigations of turbomachine cascades showed that an axial-radial diffuser with a movable backwall was not applied in experiments of cascades in the wide range of operating modes. However, the necessity for installation of such a diffuser is related to the problems of many aerodynamic test facilities when the compressor power is insufficient to get a supersonic flow downstream of the cascade. The given paper presents the experimental studies on the nozzle cascades applying an axial-radial diffuser with an axially adjustable backwall that were carried out for the first time. In addition, computational studies were performed and verified on the same channels, since the experimental results did not seem sufficient to explain all the issues related to the flow in the diffuser and its characteristics. This made it possible to split the total loss coefficient into internal losses and exit velocity losses in order to study these components separately, and also made it possible to obtain a qualitatively proper and valid flow picture and to analyze complicated issues of the flow in the diffuser, especially at supersonic modes with choke presented.

2 Experimental research

The objective of the experimental research was to develop and obtain the characteristics of the aerodynamic tunnel's operating part with a radial diffuser, which could ensure a wide range of Mach numbers (0.3–1.3) behind the annular nozzle cascade, i.e. applying supersonic modes at a relatively low (1.35–2) compressor pressure ratio. The experimental research of the annular nozzle cascade with diffusers was performed in the laboratory of Department of Turbine Construction, National Technical University "Kharkiv Polytechnic Institute" [27, 28]. The parameters of the nozzle cascade (N19, Fig. 1) are as follows: the ratio of the average diameter 175 mm to the blade's length 20 mm equals 8.75; the outlet gauging angle $\alpha_1 = 19$ deg; the number of blades is 21. The design operating mode of the cascade N19 was the operating mode with $M_{1t} = 0.95$.

Diffusers of two different designs were installed behind the nozzle. In the first experiment, a fixed annular cone-shaped diffuser was installed behind the annular cascade, similar to the research of Donovan [25]. This diffuser provided neither the required pressure decrease nor the supersonic velocity behind the annular cascade. The reason was the low expansion ratio of the diffuser, the flow separation from its hub, and the large friction surface with the outer contour (the results of this experiment are not investigated in this article).

In the second experiment, an axial-radial operating area W (section 1 – section TD) and a radial diffuser RD after it (section TD – section 2) were installed behind the annular cascade N19 (Fig. 1). The diffuser was designed with the possibility to regulate the axial position of the backwall BW (the one farther from the cascade) during the experiment.
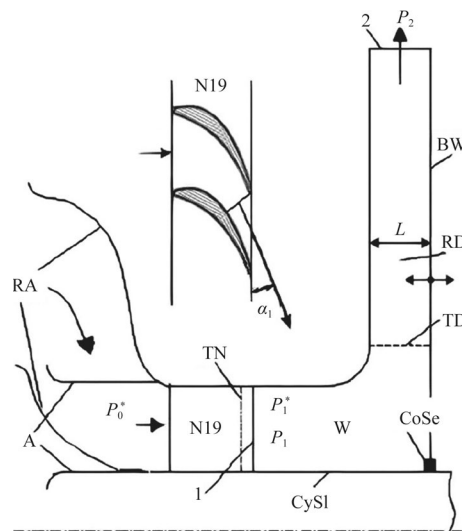
Fig. 1 Layout of the aerodynamic tunnel's operating part

The idea was based on the operation of supersonic aerodynamic tunnels with regulated diffusers for axial flow (without axial velocity component) [1, 14, 16, 17, 29], which allow to influence the shock wave position in the throat area of the diffuser to decrease the stagnation pressure loss.

We did not find any sources about regulated diffusers that are located behind the transonic annular nozzle cascades and operate in highly swirling subsonic and supersonic conditions.

In our design, the axially movable backwall BW allowed easy adjustment of the expansion ratio of the output channel ("operating part W + diffuser RD") during the operating process of the installation. The axial operating part W from section 1 till the throat TD consisted of a rather long axial part with cylindrical edges and a swivel axial part followed by a radial diffuser RD. A contact seal CoSe was located between the backwall BW and the cylinder hub (sleeve) CySl, and prevented air leaks even at a deep vacuum inside the operating part W. The geometric expansion ratio of the radial diffuser RD from the throat TD till the outlet section 2 didn't change and was equal to 2.37 as the backwall BW was moved parallel to the front wall. The geometric expansion ratio $n_{\mathrm{W+RD}}$ of the operating part W and the radial diffuser RD, i.e., the ratio of the sectional area 2 (variable) to the cross-sectional area 1 (constant), changed in direct proportion to the radial diffuser's backwall position. For example, the expansion ratio was $n_{\mathrm{W+RD}} = 1.15$, 1.79, and 2.58 for sizes $L = 8$, 12.5, and 18 mm. Hereinafter, the outlet channel W + RD is called a diffuser.

The experiments were performed with two types of entrances to the cascade nozzle N19: A + N19 + RD – with axial inlet, and RA + N19 + RD – with radial-axial inlet. The research was executed by means of two compressors: an electrically driven compressor with power of 120 kW was applied at subsonic operating modes, while for transonic modes a compressor with power of 700 kW was used, which ensured excess (gauge) stagnation pressure before the operating area up to 29 kPa and up to 95 kPa, respectively.

All pressure and stagnation pressure values are presented in this article as excess (gauge) ones.

Total loss coefficient ζ_{ol} was calculated for the entire channel, located behind the annular cascade, which consisted of an operating area and a radial diffuser "W + RD" (Fig. 1):

$$\zeta_{ol} = \frac{1 - \left[(P_2 + B)/\left(P_{1m}^* + B\right)\right]^{\frac{k-1}{k}}}{1 - \left[(P_1 + B)/\left(P_{1m}^* + B\right)\right]^{\frac{k-1}{k}}}.$$

Where k is the working fluid isentropic exponent, B is the barometric pressure, P_1 and P_2 are the pressure in sections 1 and 2 respectively ($P_2 = 0$, P_1 is half of the sum of the peripheral and hub drain indicators in section 1), and P_{1m}^* is the circumferentially averaged stagnation pressure at the mean radius of section 1.

The following formula was used to calculate the absolute stagnation pressure behind the cascade:

$$P_{1m}^* + B = \sigma_m\left(P_0^* + B\right),$$

where $\sigma_m = \left[\frac{1 - \frac{k-1}{k+1}\lambda_{1t}^2}{1 - \frac{k-1}{k+1}\lambda_{1t}^2(1-\zeta_{nm})}\right]^{\frac{k}{k-1}}$, ζ_{nm} is the kinetic energy loss coefficient at the mean cascade radius [28], and

$$\lambda_{1t} = f\left(P_0^*, P_1, k\right).$$

Figures 2, 3 and 4 show the dependency of the total loss coefficient ζ_{ol} and the Mach number M_{1t}, which were obtained while testing a compressor of 120 kW power.

At the operating mode of almost maximum compressor head, where the stagnation pressure before the cascade P_0^* reached 28.0 kPa, the L value varied between 8 and 18 mm (Fig. 1) by shifting the back wall in the axial direction. The optimum position of the wall had been defined as equal to 10 mm (Fig. 2). In this position of the wall and under a constant stagnation pressure of $P_0^* = 28.0$ kPa before the annular cascade, the total loss coefficient ζ_{ol} and the pressure behind the nozzle P_1 had the minimum values of 0.446 and -27.80 kPa, respectively, while the averaged theoretical Mach number M_{1t} in section 1 reached the value of 0.94 (Fig. 4). At $L = 10$ mm, the influence of the Mach number M_{1t} on the total loss coefficient of the channel W + RD was also investigated (the stagnation pressure P_0^* changed from 2.5 to 28.0 kPa). It was found (Fig. 3) that the change of Mach number within the subsonic range did not affect significantly on the coefficient ζ_{ol}.

At $P_0^* = 28.0$ kPa, shifting the diffuser wall up to 18 mm considerably increased the loss coefficient ζ_{ol}. As a result of increasing the pressure P_1 up to -13.60 kPa, the Mach number M_{1t} behind the nozzle decreased to 0.84 (Fig. 4). Despite the reduced operating performance, the diffuser had a good regenerative capacity that allowed keeping vacuum behind the nozzle as well as the high Mach number M_{1t} over the whole investigated range of the wall position L at subsonic modes. Reducing L to 8 mm led to a slight decrease of M_{1t}.
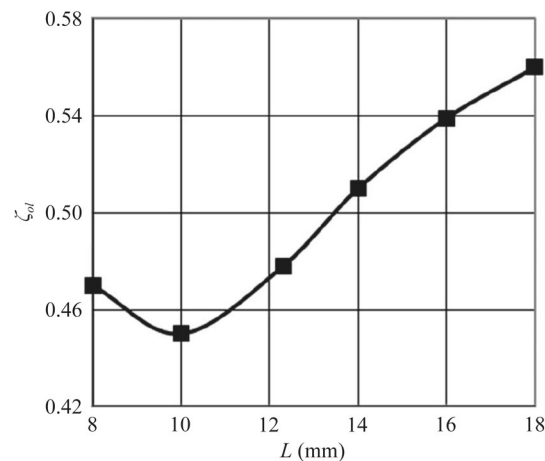
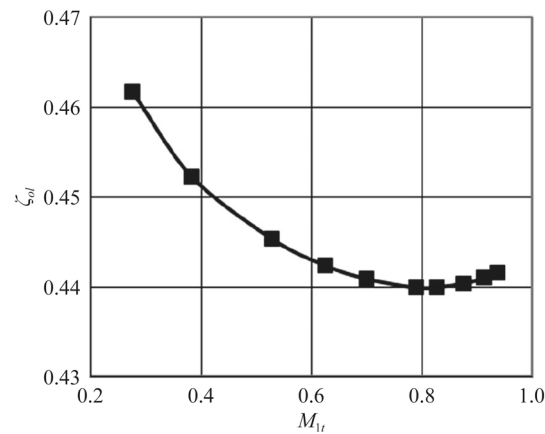Fig. 2 Influence of size L on coefficient ζ_{ol} at $P_0^* \approx 28.0$ kPa

Fig. 3 Influence of Mach number M_{1t} on coefficient ζ_{ol} at $L = 10$ mm and $P_0^* = 2.5$–28.0 kPa

If a transition duct with support struts was installed instead of a radial diffuser while using the 120 kW compressor, then the pressure P_0^* increased up to 31 kPa, the pressure P_1 increased up to zero, and the Mach number M_{1t} decreased to 0.63. Thereby, when using a 120 kW supercharger, it was only possible to reach the design operating mode of the nozzle cascade $M_{1t} = 0.95$ by applying a radial diffuser, which had an expansion ratio $n_{W+RD} = 1.43$ ($L = 10$ mm). In this mode at $P_0^* = 28.0$ kPa, $T_0^* = 313$ K, $G = 0.997$ kg/s, the N19 cascade had a minimum kinetic energy loss coefficient $\zeta_{nm} = 0.045$. Momentary kinetic flow energy behind the cascade was equal to 50 kW. Ideally, the natural conditions behind the nozzle cascade could be provided by means of an operating cascade, which had a rotational speed of 2500 rpm and had a relative flow angle at the mean diameter $\beta_1 = 60$ deg. However, in both cases the radial pressure gradient dP/dr was 1.4 times higher than $\rho_1 C_{1u}^2/r$, which allowed for performing the research of the nozzle cascade without a rotor blade.

The research performed with a 700 kW compressor at sub- and supersonic modes showed that choke modes can occur at $L = 10$ mm in an enclosed wind tunnel, when a
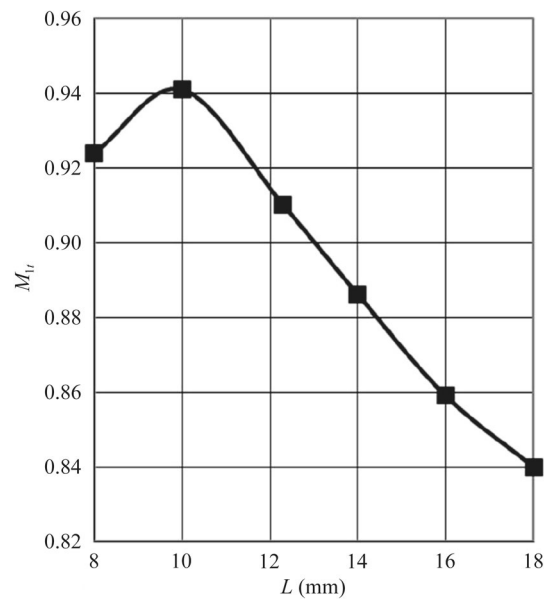
Fig. 4 Influence of size L on Mach number M_{1t} at $P_0^* \approx 28.0$ kPa

pressure increase before the nozzle cascade doesn't change the Mach number behind the cascade, and the total loss coefficient ζ_{ol} of the $W + RD$ channel increases dramatically. The operating mode, at which the choke in channel $W + RD$ occurs, was affected by the position of the radial diffuser's backwall with respect to the front one. Figure 5 shows the dependency $M_{1t} = f\left(P_0^*, L\right)$ at two types of air entrance into the nozzle cascade: one with a radial-axial inlet (RA) – $RA + N19 + RD$, and the other one with an axial inlet (A) – $A + N19 + RD$. The $A + N19 + RD$ option was investigated at $L = 10$ mm only.

Analysis of the dependency plot in Fig. 5 led to the following conclusions:

1. At operating modes with $M_{1t} < 1.1$, the construction of the entrance section didn't influence the Mach number;
2. At $L = 10$ mm ($n_{W+RD} = 1.43$), the diffuser was chocked in the $A + N19 + RD$ case at $P_0^* \approx 5500$ kg/m^2 and $M_{1t} = 1.16$. There is a slight tendency for the Mach number to decrease to 1.147 as the pressure increases up to 9500 kg/m^2.
3. At $L = 10$ mm and $P_0^* \approx 8000$ kg/m^2, a replacement of the radial cascade entry with a radial-axial one (switch from option $A + N19 + RD$ to option $RA + N19 + RD$) led to an increase in the Mach number M_{1t} from 1.16 to 1.24. However, at such a small L and a high pressure P_0^*, the diffuser's reducing capacity probably reached its limit, hence L should be increased.
4. If pressure P_0^* produced by the 700 kW compressor is higher than 5000 kg/m^2, it's reasonable to eliminate the diffuser's choke modes through increasing L up to 11–12.5 mm ($n_{W+RD} = 1.57$–1.79). The maximum Mach numbers $M_{1t} = 1.34$ and 1.38 were obtained at the length $L = 12.5$ mm and stagnation pressure $P_0^* = 7900$ and 9000 kg/m^2, respectively.
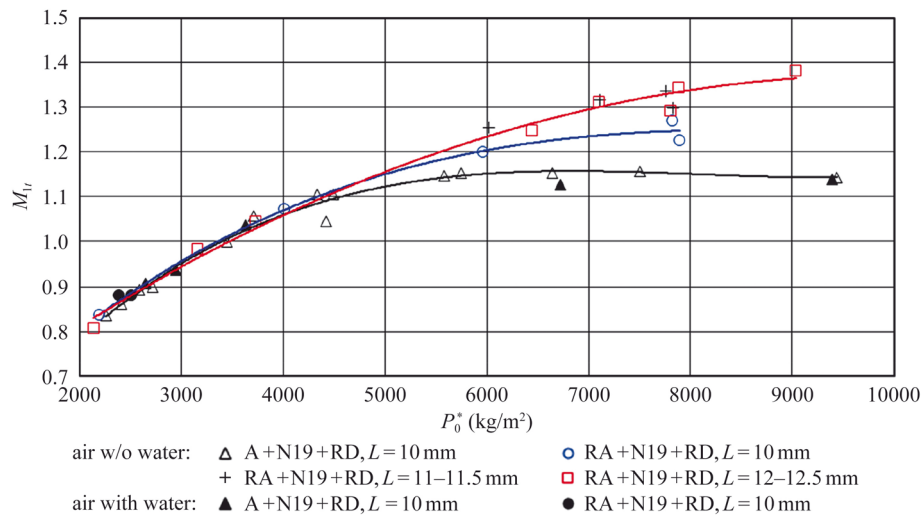
Fig. 5 Influence of P_0^* and size L on Mach number M_{1t}

Since the increase of M_{1t} from 1.34 to 1.38 did not lead to either the reduced (corrected) flow rate change $G\sqrt{T_0^*}/(P_0^* + B)$ or the flow coefficient change, the nozzle cascade was completely chocked. Confirmation of that is the absence of supersonic velocities within the control section 1 behind the cascade. The measurements of stagnation pressure P_1^* and flow outlet angle α_1 at 49 points of section 1 were performed using an orientable Pitot tunnel with a diameter of 0.8 mm. The flow pressure was measured at the stage endwalls using drains, and it was considered constant in the tangential direction and was equal to -6170 kg/m^2 at the hub (an annular drain) and -1780 kg/m^2 at the tip (eight drains).

The horizontal part of the function $M_{1t} = f(P_0^*, L)$ in Fig. 5 is corresponded by the vertical part of the function $\zeta_{ol} = f(M_{1t}, L)$ in Fig. 6, which indicates the critical rise of losses and diffuser choke at $L = 10$ mm.

At $L = 12.5$ mm, the diffuser's total loss coefficient did not exceed 0.58 even at extremely high Mach numbers, and decreased monotonously to 0.45 when the Mach number reduced to 0.6. The size $L = 12.5$ mm was optimal at the pressure of about 79 kPa (Fig. 7). For a rational use of 120 kW compressor capacities at limiting pressure of 29 kPa and a flow rate of 1.05 kg/s, a diffuser with a wall position $L = 10$ mm should be used (Fig. 2). The higher the pressure before the cascade, the higher the diffuser's optimum expansion ratio (Fig. 7).

Therefore, the developed vaneless annular channel with an adjustable radial diffuser allowed a rational use of the compressor equipment capacities and gave the possibility to perform research on turbines' annular nozzle cascades at both subsonic and supersonic operating modes. The optimum positions of the radial diffuser back wall were determined to ensure the minimum total loss coefficient of the channel W + RD and, accordingly, the maximum possible Mach number behind the tested cascade with fixed constant pressure at the cascade inlet.

The hydraulic resistance of models A + N19 + RD and RA + N19 + RD was mainly determined by the losses within the diffuser. And so, when using the 700 kW compressor at operating limits, the L size reduction from 12.5 mm to 10 mm led to the diffuser
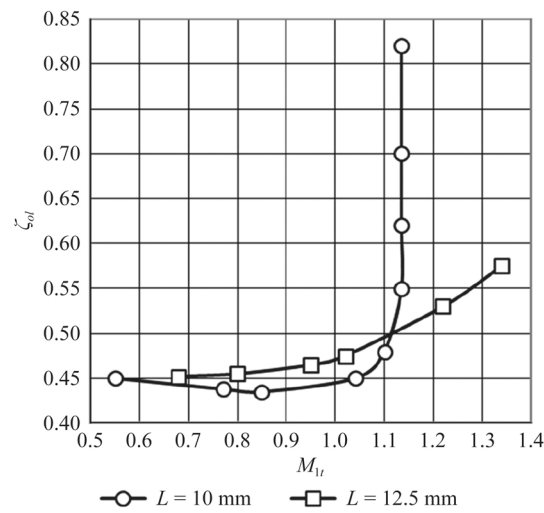
Fig. 6 Influence of size L on dependence of factor ζ_{ol} on Mach number M_{1t}
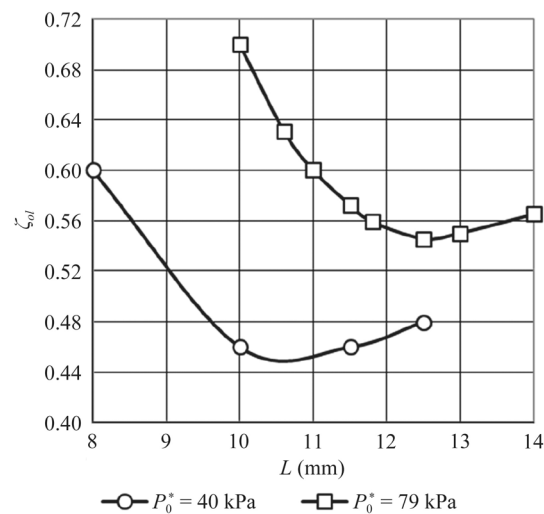

Fig. 7 Influence of stagnation pressure P_0^* on dependence of factor ζ_{ol} on size L

choke, increasing ζ_{ol} from 0.58 to 0.8 and reducing Mach number M_{1t} from 1.38 to 1.147. At the same time, the stagnation pressure before the nozzle cascade increased from 9000 to 9500 kg/m^2.

3 Computational studies

The experimental studies showed that the developed installation is reasonable in terms of stable operation at different modes, however, the computational research is necessary to obtain a more detailed flow picture to analyze complicated problems related to the flow in the diffuser and its characteristics at various operating modes. In this study, the Reynolds-Averaged Navier-Stokes equations were solved using the commercial CFD solver ANSYS Fluent. Computational studies of an axisymmetric channel W + RD were performed without a nozzle cascade at the inlet (Figs. 8 and 9). An axisymmetric model allows both a significant reduction in the number of mesh

elements and a reduction in the time taken to obtain results, which is very important for perspective optimization tasks of the design of the outlet channels that operate in a highly swirling flow. The calculations using density-based solution methods were performed for four variants of computational models using CFD. The models differed in the distance L from the front to the backwall of the diffuser radial part − L was equal to 8 mm, 10 mm, 12.5 mm and 18 mm. The local mesh refinement near the diffuser walls was set so that to ensure that the boundary layer factor $Y+$ was close to 1. The Spalart–Allmaras turbulence model with specifying modified turbulence viscosity and applying vorticity-based production was used, which was tested earlier in diffuser calculations [30], and fit experimental data well for unseparated, pre-separated and separated diffusers compared to the other known turbulence models from the Fluent database.

The objectives of the computational study included the following: to define the dependencies of the total loss coefficient, the internal loss coefficient, and the exit velocity losses on the Mach number M_1; to study the flow nature within the $W+RD$ channel in a wide range of Mach number values, including the choke modes; to compare the computational and experimental data to determine the possibility of the $W+RD$ channel investigation in a highly swirling flow simulation at the inlet applying an axisymmetric flow model.

The control sections 1, TD and 2 of the $W+RD$ channel were placed in the computational model in the same way as in the experimental model. A specially designed inlet preliminary (preparatory) axial-radial-axial converging region (section 0 − section 1) was used instead of the nozzle cascade before the $W+RD$ channel. This allowed the simulation of the flow parameter distribution behind the nozzle cascade in section 1 similarly to the experimental one without using a 3D nozzle cascade model.
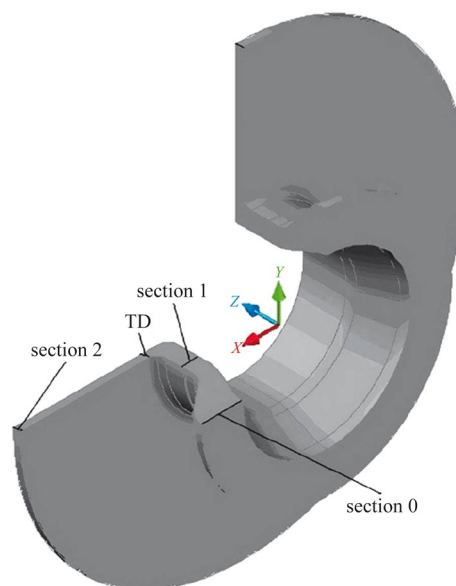

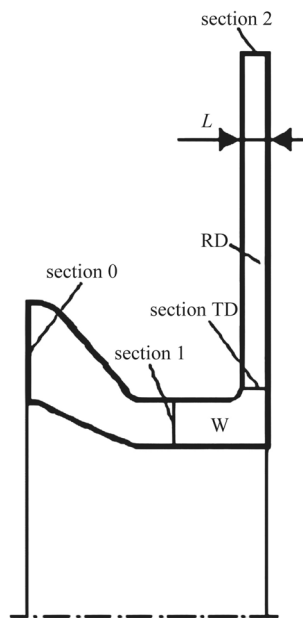**Fig. 8** Axisymmetric computational model of the diffuser

Fig. 9 Meridional view of the diffuser computational model

Three loss coefficients of the W + RD channel were calculated:

a)   total loss coefficient

$$\zeta_{ol} = \frac{1 - \left[(P_2 + B)/\left(P_1^* + B\right)\right]^{\frac{k-1}{k}}}{1 - \left[(P_1 + B)/\left(P_1^* + B\right)\right]^{\frac{k-1}{k}}}.$$

b)   exit velocity loss coefficient

$$\zeta_{ev} = \frac{1 - \left[(P_2 + B)/\left(P_2^* + B\right)\right]^{\frac{k-1}{k}}}{1 - \left[(P_1 + B)/\left(P_1^* + B\right)\right]^{\frac{k-1}{k}}}.$$

c)   internal loss coefficient (hydraulic losses)

$$\zeta = \zeta_{ol} - \zeta_{ev}.$$

Here, P_2^* is the excess (gauge) stagnation pressure in section 2. All pressures were mass flow averaged.

Dividing of the total loss coefficient into components showed that the main portion is an internal loss coefficient, which replicates the dependency $\zeta_{ol} = f(M_1)$ almost equidistantly, except for the diffuser choke modes (Figs. 10, 11, 12 and 13). The internal loss coefficient ζ was significantly higher than the exit velocity loss coefficient ζ_{ev} that was equal to 0.1–0.14 at almost all operating modes. The difference of these factors $\Delta\zeta = \zeta - \zeta_{ev}$ increased by a factor of 2.5–3.0 in subsonic and 3.0–4.5 in supersonic modes while L increased from 8 to 18 mm. In the choke modes of the channel, which were obtained at $L=8$ mm and $L=10$ mm within the pressure range investigated, the total loss coefficient growth also occurred mainly due to internal losses.

Based on the loss coefficient dependencies on the M_1 number (Figs. 10, 11, 12 and 13), it can be concluded that the W + RD channel is very sensitive to the diffuser backwall position both in the experiment and in the calculation.

At the minimum size $L=8$ mm in the Mach number range $M_1=0.55-0.9$ (when the stagnation pressure P_0^* is < 30 kPa), the loss coefficients ζ_{ol}, ζ, and ζ_{ev} almost did
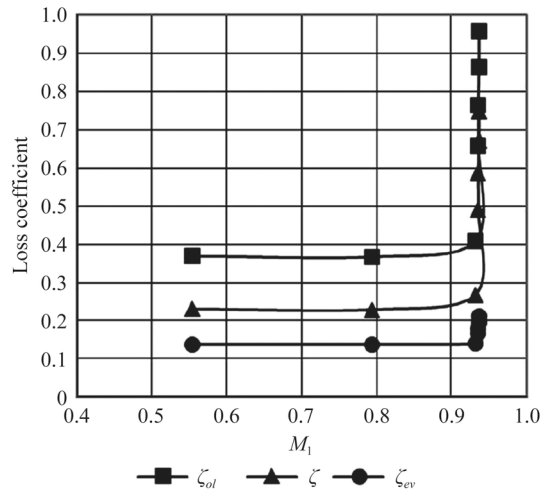

Fig. 10 Influence of M_1 on loss coefficient at $L=8$ mm
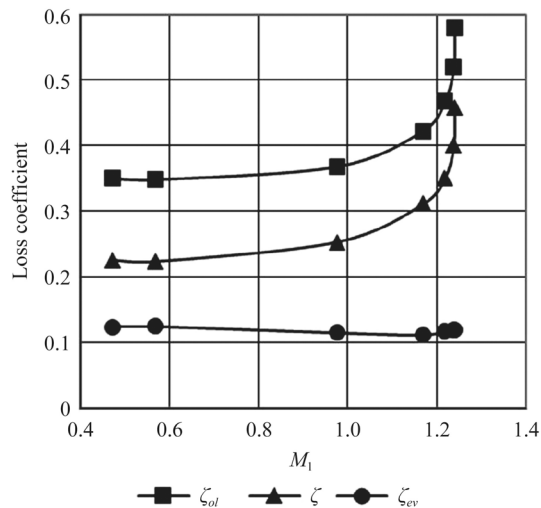

Fig. 11 Influence of M_1 on loss coefficient at $L=10$ mm
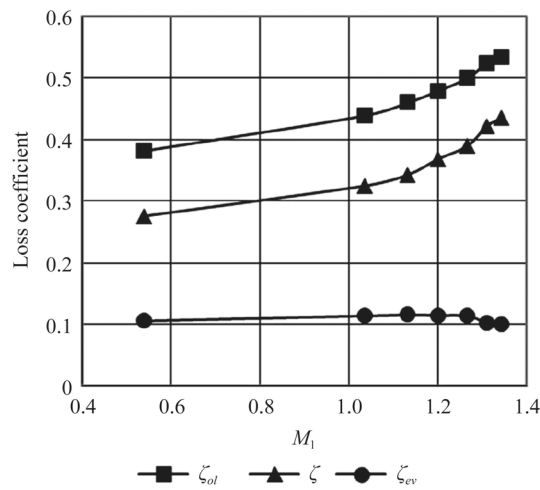
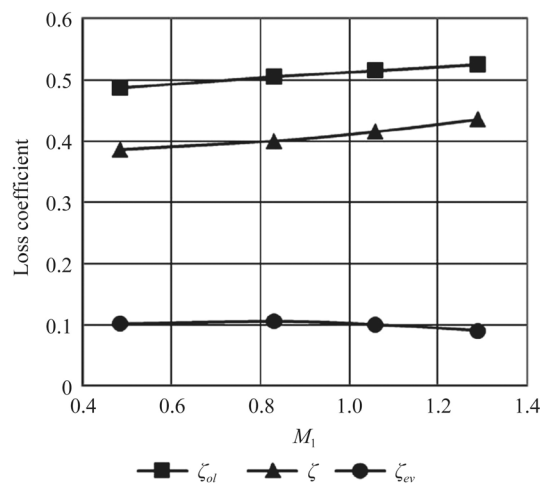**Fig. 12** Influence of M_1 on loss coefficient at $L = 12.5$ mm

Fig. 13 Influence of M_1 on loss coefficient at $L = 18$ mm

not change and remained as 0.37, 0.23, and 0.14, respectively. When the stagnation gauge pressure at inlet P_0^* was higher than 30 kPa, the blockage of the flow in the channel occurred: the Mach number M_1 did not go higher than 0.937, and the total loss coefficient increased sharply, reaching 0.958 at $P_0^* = 80$ kPa (Fig. 10, Table 1). The stagnation pressure P_1^* and the pressure P_1 increased simultaneously at the control section 1, while the Mach number M_1, the velocity components C_{1a}, C_{1u} and the flow angle α_1 remained unchanged (Table 1).

The increase of size L influenced the level of the loss coefficients and the nature of the dependency $\zeta_{ol} = f(M_1)$. When L increased up to 10 mm, the blockage mode of the channel occurred at Mach number $M_1 = 1.24$, and when L was higher than 12.5 mm, then no channel blockage was detected within the tested pressure range.

Table 1 Average parameters in case $L = 8$ mm

P_0^*, kPa	P_1^*, kPa	P_1, kPa	C_{1a}, m/s	C_{1u}, m/s	α_1, deg.	M_1
10	7.96	−12.74	65.0	196.7	18.3	0.553
20	16.09	−24.19	97.6	271.5	19.8	0.794
30	24.79	−29.75	118.4	309.7	20.9	0.932
50	44.05	−19.12	118.8	310.7	20.9	0.936
60	54.58	−14.21	119	311	20.9	0.937
70	63.29	−8.37	119	311	20.9	0.937
80	72.95	−2.94	119	311	20.9	0.937
C_{rTD}, m/s	C_{uTD}, m/s	α_{TD}, deg.	M_{TD}	ζ_{ol}	ζ	ζ_{ev}
136.5	155.6	41.3	0.553	0.369	0.231	0.139
219.2	217	45.3	0.858	0.367	0.229	0.138
328	247	53	1.212	0.408	0.268	0.141
358.9	249.3	55.2	1.318	0.655	0.490	0.165
368	248.2	56	1.347	0.764	0.585	0.179
368	248.4	56	1.348	0.863	0.669	0.194
368	248.5	56	1.348	0.958	0.747	0.211

4 Comparison of calculated and experimental data

4.1 Distribution of parameters in the channel

The obtained result data from the experimental and computational studies were compared to have a verified computational model and ensure that it gives a qualitatively proper and valid picture of the flow in the channel. The comparative distribution of parameters, obtained from the experiment behind the nozzle cascade and through the calculation without cascade in section 1, is presented for one of channel W + RD tested cases, where size $L = 12.5$ mm at the operating mode of $P_0^* = 79$ kPa, $M_{1t} = 1.34$, and $\alpha_1 \approx 20$ deg. The inlet preliminary (preparatory) region in an axisymmetric model satisfactorily simulated the distribution of the main parameters along the radius (Fig. 14). Minor differences between the calculation and the experiment were caused by the profile and end losses in the nozzle cascade and by the quite significant tangential non-uniformity of the flow parameters behind the nozzle cascade. For instance, the α_1 angle changed from −25 deg. to 73 deg. and the kinetic energy loss coefficient ζ_{nk} reached 0.38 at a distance of 0.9 mm from the hub endwall in the region of the channel vortices. Radial pressure gradient dP/dr behind the nozzle cascade in this operating mode was 1.5 times higher than $\rho_1 C_{1u}/r$, and the flow in the computational model corresponded to the simplified radial equilibrium equation $\frac{dP}{dr} \approx \frac{r C_{1u}^2}{2}$.

Considering the predominant growth of the velocity flow component over its tangential component in the confuser area from section 0 to section 1, the inlet flow angle in section 0 was set 3–3.5 times lower than the α_1 angle, which had to be obtained in the control section 1, depending on the flow conditions.

4.2 Influence of size L on diffuser operation

During experimental and computational studies, different locations of the regulated backwall of the diffuser at various operating modes were investigated, and the influence of the size L on the diffuser operation was studied. The objective was to define
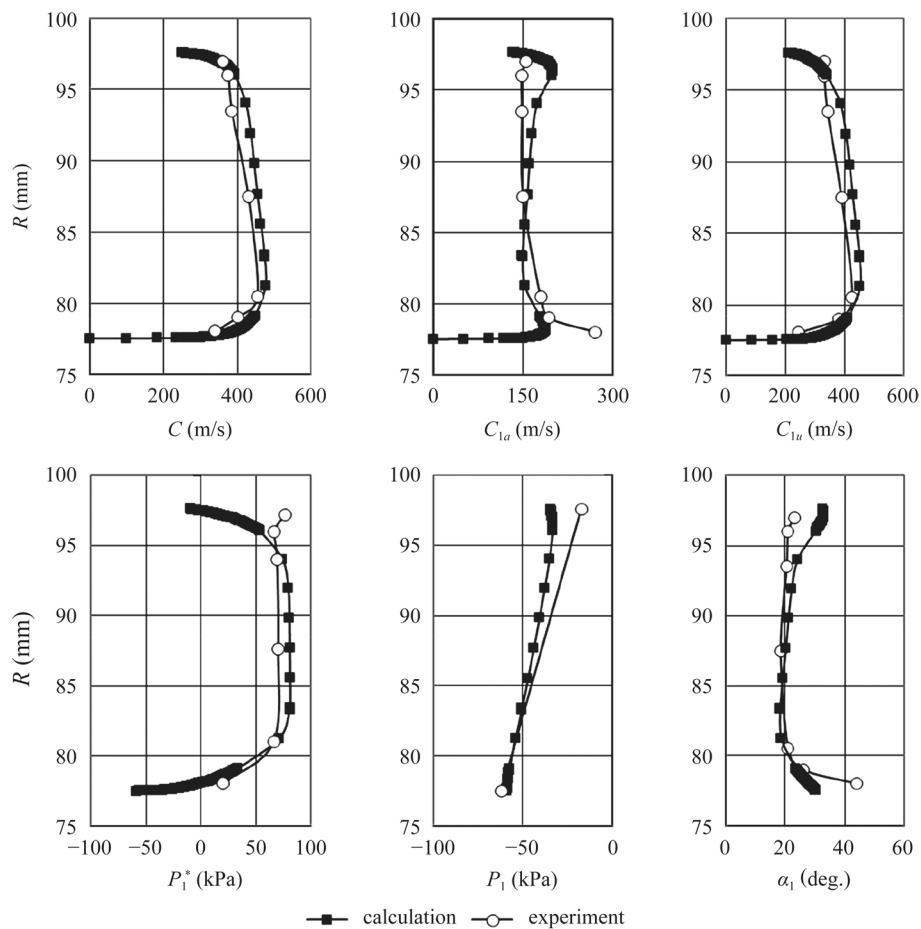
Fig. 14 Distribution of parameters at section 1 in calculation and experiment of variant with $L = 12.5$ mm at $P_0^* = 79$ kPa, $M_{1t} = 1.34$, and $a_1 \approx 20$ deg.

the optimum expansion ratio of the output channel located behind the cascade for each operating mode of the annular cascade. For a correct comparison of the calculated and experimental data, the latter were represented by the coordinates M_1 and ζ_{ol}. An average Mach number $M_1 = M_{1t} \cdot \sqrt{1 - \zeta_n}$ was used instead of the theoretical one M_{1t}, where ζ_n stands for an integral loss coefficient in the nozzle cascade. Reducing the factor σ with respect to factor σ_m led to the decrease of the pressure $P_1^* + B$ comparatively to pressure $P_{1m}^* + B$ and the total loss coefficient of the diffuser ($\zeta_{ol} < \zeta_{ol\ mid}$).

In the experiment with $L = 10$ mm, the diffuser in the variant of $A + N + RD$ was chocked at $P_0^* \approx 55$ kPa, $M_{1t} = 1.16$, and $M_1 = 1.11$, which resulted in a critical rise of the total loss coefficient (Figs. 15 and 16). In turn, this diffuser had lower losses in the calculations, as depicted in Fig. 15, and thus was chocked at a higher Mach number $M_1 = 1.24$. That is why it makes sense to increase the roughness degree of the diffuser walls in the calculations in order to raise the hydraulic loss coefficient, which is the main component of the total losses (Fig. 11). For the limit value of $M_{1t} = 1.38$ and $M_1 = 1.3$, a diffuser with $L = 12.5$ mm is the optimal one. Figure 15 indicates that the calculation method makes it possible to precisely find the optimum range of
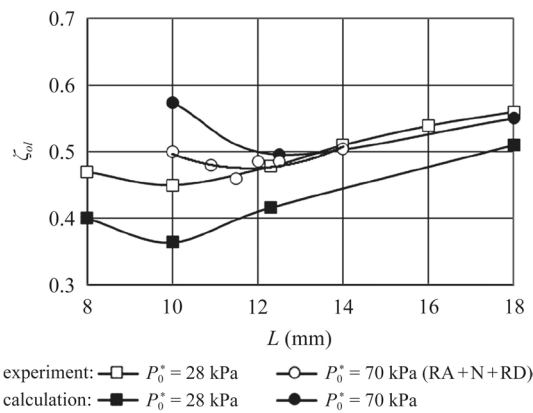
Fig. 15 Influence of size L on coefficient ζ_{ol} at $P_0^* \approx 28$ kPa and 70 kPa
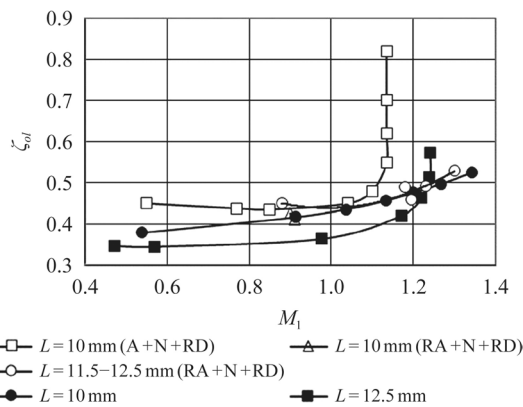

Fig. 16 Influence of Mach number M_1 on coefficient ζ_{ol} at $L = 10$ mm and 12.5 mm

the diffuser expansion ratio, though it underestimates the level of losses within this range.

To summarize it, the designed vaneless inlet section (area) allowed the satisfactory modelling of the flow structure behind the nozzle cascade and the determination of the diffuser characteristics without applying a nozzle cascade in the computational model, and made it possible to apply an axisymmetric model in the CFD calculations, which significantly reduced the time of the rather extensive calculations.

5 Flow structure analysis in diffuser with $L = 8$ mm

A detailed analysis of the calculation model work with a minimum diffuser expansion ratio in a wide range of operating modes is of specific interest, since such a channel is choked at the lowest stagnation pressure P_0^*. The average data values in the case of $L = 8$ mm are presented in Table 1, where: P_0^* is the stagnation pressure in section 0; P_1^* and P_1 are the flow averaged stagnation pressure and static pressure in section 1; C_{1a}, C_{1u}, α_1, and M_1 are the flow averaged axial, tangential velocity components, flow angle, and Mach number in section 1; C_{rTD}, C_{uTD}, α_{TD}, and M_{TD} are the flow averaged radial, tangential velocity components, flow angle, and Mach number in section TD; ζ_{ol} is the total loss coefficient, ζ is the internal (hydraulic) loss coefficient, and ζ_{ev} is the exit

velocity loss coefficient. At $M_1 = 0.937$, the stagnation pressure loss coefficient in the region between sections 0 and 1 was almost the same as the one with applying a nozzle cascade.

When analyzing the swirled flow, the major focus should not be on the Mach numbers M_1 and M_{TD}, but on the flow component of the velocity. The tangential component only intensifies the process of kinetic energy dissipation in the annular channel. As depicted in Table 1, a diffuser with $L = 8$ mm was chocked at pressure $P_0^* \approx 55$ kPa, when the flow component of Mach number $M_{rTD} = M_{TD} \cdot \sin(\alpha_{TD})$ in its throat section was slightly higher than one.

When the stagnation pressure P_0^* at the inlet increased from 10 to 30 kPa, the pressure P_1 in section 1 decreased to its minimum, while the Mach number M_1 rose from 0.553 to 0.932, and M_{TD} increased from 0.553 to 1.212 in section TD. When the stagnation pressure P_0^* became higher than 55 kPa, the flow was chocked in the W + RD channel. The flow kinematics in the channel W did not change within the studied pressure range $P_0^* = 60$–80 kPa, as pressure P_1 proportionally increased with the rise of the stagnation pressure P_1^*. Based on Table 1, the velocity and flow angles remain unchanged within this pressure range in the control sections 1 and TD. At the same time, the flow velocity in this region increased from 332 to 444 m/s, the flow component of the velocity increased from 119 to 368 m/s, and the sonic line was located before section TD.

In the region between sections 1 and TD, the flow swirl significantly decreased by 22 deg. at the pressure of 10 kPa, and by 35 deg. at operating modes where the diffuser was chocked. At $P_0^* = 10$ kPa, the flow density was almost constant, which is why narrowing the flow passage of the channel "1-TD" by two times increased the flow component of velocity as twice. The tangential component of the velocity decreased by 1.26 times due to its interaction with the channel walls, though the radius of section TD was 1.21 times greater than the mean radius of section 1. At high flow velocities, its compressibility does not have much influence on the ratio of the tangential velocity components C_{uTD}/C_{1u}; however, it significantly increased the ratio of the flow velocity components C_{rTD}/C_{1a} from 2 to 3, which led to growth in the angle difference $\alpha_{TD} - \alpha_1$ to 35 deg.

With pressure growth from 50 to 80 kPa, the main changes in the flow structure occurred behind the throat section TD in the radial diffuser RD. As the stagnation pressure P_0^* increased, the region in the inlet section of the radial diffuser RD, where the pressure and flow density decreased, increased in size and, therefore, the flow velocity and Mach number grew. At the stagnation pressure $P_0^* = 80$ kPa, the size of this region increased to 30 mm, if measured from section TD, and the gauge pressure decreased to -77 kPa, while the Mach number increased to 1.9. A shock wave closed this region, which was followed downstream by a drastic pressure increase and a velocity decrease. Fluctuating wavy processes with local regions of flow acceleration took place here (Figs. 17, 18 and 19).

6 Conclusions

1. In order to model the radial pressure gradient behind the annular cascades of a medium diameter to blade height ratio ($D/l = 5$–9), a cylindrical working area and a radial diffuser should be installed behind them.
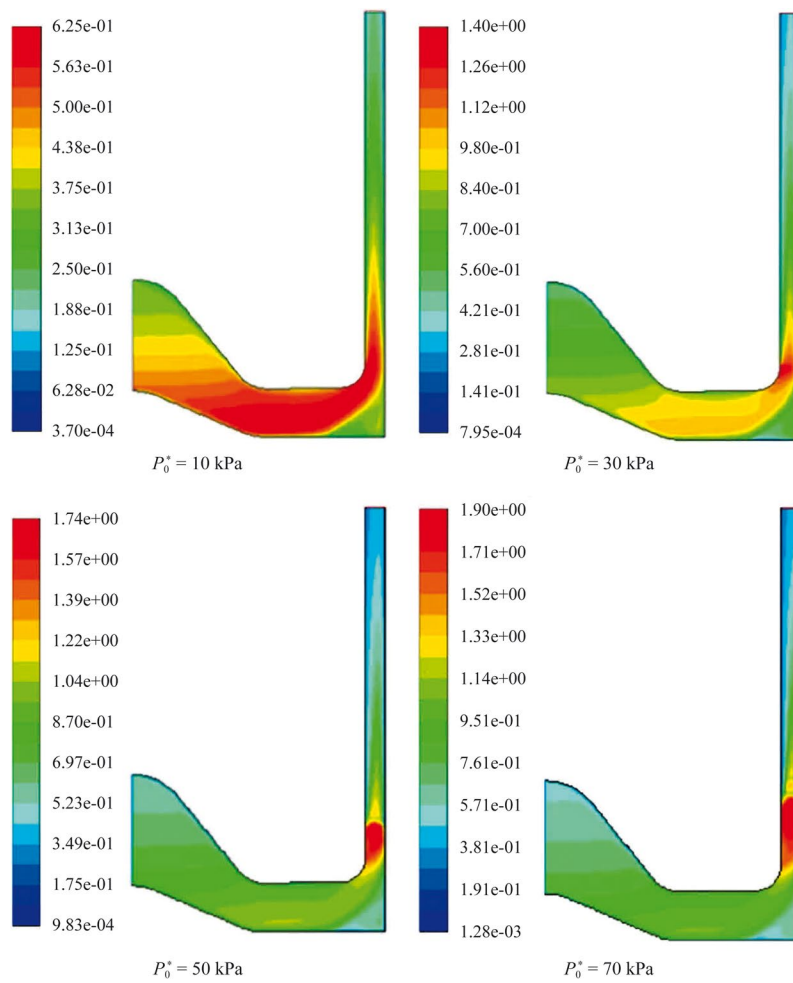
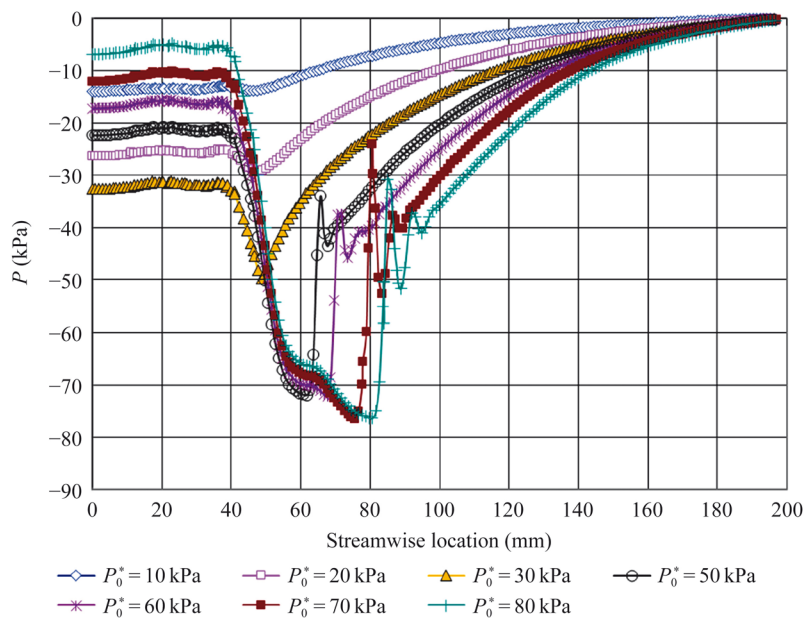**Fig. 17** Distribution of Mach number in case of $L = 8$ mm with different stagnation gauge pressure at inlet P_0^*

Fig. 18 Pressure distribution along the mean streamline in case of $L = 8$ mm
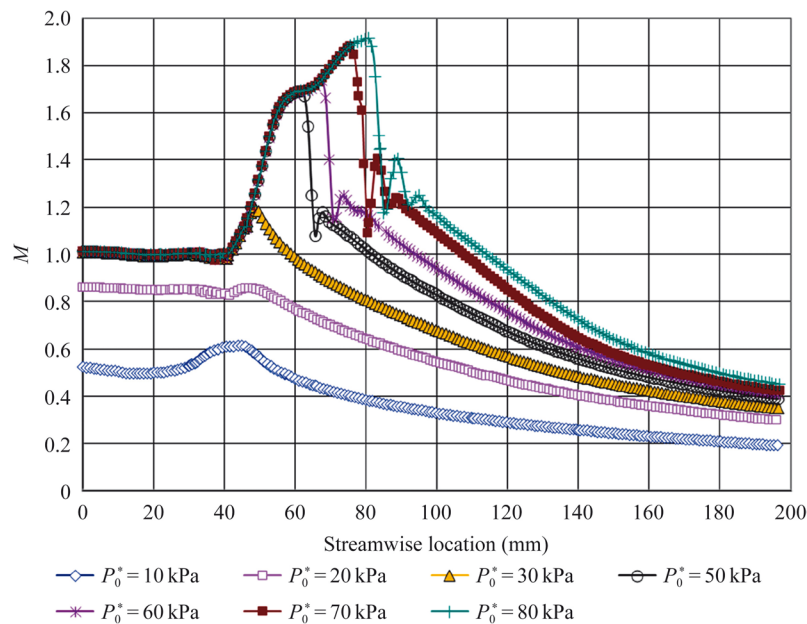
Fig. 19 Mach number distribution along the mean streamline in case of $L = 8$ mm

2. An optimum expansion ratio of the output channel located behind the cascade was determined for each operating mode of the annular cascade both by calculation and by experiment. As the Mach number at the cascade outlet increases, the diffuser wall should be moved, thereby increasing the flow passage area. If the position of the diffuser wall that is defined as optimum for subsonic modes is fixed, then a flow choke mode can occur in the converging–diverging outlet channel behind the annular turbine cascade at supersonic modes.

3. It was determined that the shape of the vaneless channel before the nozzle cascade does not influence the flow structure behind the cascade and the diffuser operating at subsonic modes. However, replacing the annular cascade entrance by a radial-axial one at supersonic modes with $M_{1t} > 1.1$ substantially changes the flow structure, which increases the diffuser efficiency.

4. During the CFD calculations of the computational model, it is possible not to use a turbine cascade, but instead apply a vaneless inlet converging area section, which allows performing calculations with an axisymmetric formulation, and satisfactory results can be obtained, while significantly reducing the time of the rather extensive calculations. This computational model can be used to optimize the design of an aerodynamic tunnel outlet area.

Declarations

References

1. Hirsch C, Sieverding CH (1993) Types of cascade tunnels (continuous, blow down/suction, short duration open closed loop) and references to existing literature on instrumentation. In: Hirsch C (ed) Advanced methods for cascade testing. NATO Research and Technology Organisation, Paris
2. Arisi AN (2016) Heat transfer and flow characteristics on the rotor tip and endwall platform regions in a transonic turbine cascade. Dissertation, Virginia Polytechnic Institute and State University
3. Anto K, Xue S, Ng WF et al (2013) Effects of tip clearance gap and exit Mach number on turbine blade tip and near-tip heat transfer. In: Proceedings of the ASME turbo expo 2013: turbine technical conference and exposition. Vol 3C: heat transfer, San Antonio, 3-7 June 2013. https://doi.org/10.1115/GT2013-94345
4. Holmberg DG, Diller TE (2005) Simultaneous heat flux and velocity measurements in a transonic turbine cascade. J Turbomach 127(3):502–506. https://doi.org/10.1115/1.1860576
5. Nix AC, Diller TE, Ng WF (2007) Experimental measurements and modeling of the effects of large-scale freestream turbulence on heat transfer. J Turbomach 129(3):542–550. https://doi.org/10.1115/1.2515555
6. Smith DE, Bubb JV, Popp O et al (2000) An investigation of heat transfer in a film cooled transonic turbine cascade: Part I — steady heat transfer. In: Proceedings of the ASME turbo expo 2000: power for land, sea, and air. Vol 3: heat transfer; electric power; industrial and cogeneration, Munich, 8-11 May 2000. https://doi.org/10.1115/2000-GT-0202
7. Popp O, Smith DE, Bubb JV et al (2000) Investigation of heat transfer in a film cooled transonic turbine cascade: Part II — unsteady heat transfer. In: Proceedings of the ASME turbo expo 2000: power for land, sea, and air. Vol 3: heat transfer; electric power; industrial and cogeneration, Munich, 8–11 May, 2000. https://doi.org/10.1115/2000-GT-0203
8. Carullo JS, Nasir S, Cress RD et al (2011) The effects of freestream turbulence, turbulence length scale, and exit Reynolds number on turbine blade heat transfer in a transonic cascade. J Turbomach 133(1):011030. https://doi.org/10.1115/1.4001366
9. Nasir S, Carullo JS, Ng WF et al (2009) Effects of large scale high freestream turbulence and exit Reynolds number on turbine vane heat transfer in a transonic cascade. J Turbomach 131(2):021021. https://doi.org/10.1115/1.2952381
10. Jeffries MS (1994) The commissioning and enhancement of a blow down wind tunnel. Dissertation, Carleton University
11. Jeffries MS, Sjolander SA (1995) The Carleton University high-speed wind tunnel. In: Proceedings of the CASI 7th symposium on propulsion, Canadian Aeronautics and Space Institute, Montreal, 1995
12. Corriveau D (2005) Influence of loading distribution on the performance of high pressure turbine blades. Dissertation, Carleton University
13. Sooriyakumaran CAR (2014) Experimental study of profile losses in three transonic turbine cascades. Dissertation, Carleton University
14. Stepanov G (1962) Hydrodynamics of turbomachine cascades. Fizmatgiz, Moscow
15. Kodzwa PM Jr, Vicharelli A, Medic G et al (2009) Evaluation of alternatives for two-dimensional linear cascade facilities. J Turbomach 131(3):031001. https://doi.org/10.1115/1.2985073
16. Deych MY, Philipp G, Lazarev L (1965) Atlas of the cascade profiles of axial-flows turbine. Mashinostroyeniye, Moscow
17. Gostelow JP (1984) Cascade aerodynamics. Pergamon Press, Oxford
18. Goldman LJ, McLallin KL (1977) Effect of endwall cooling on secondary flows in turbine stator vanes. In: AGARD 49th propulsion and energetics panel conference, The Hague, 28 March - 4 April 1977
19. Williamson RG, Moustapha SH (1986) Annular cascade testing of turbine nozzles at high exit Mach numbers. J Fluids Eng 108:313–320. https://doi.org/10.1115/1.3242579
20. Govardhan M, Venkatrayulu N, Prithvi Raj D (1986) Secondary losses in a large deflection annular turbine cascade: effect of the entry boundary layer thickness. In: Proceedings of the ASME 1986 international gas turbine conference and exhibit. Vol 1: turbomachinery, Dusseldorf 8-12 June 1986. https://doi.org/10.1115/86-GT-171
21. Williamson RG, Moustapha SH, Huot JP (1986) The effect of a downstream rotor on the measured performance of a transonic turbine nozzle. J Turbomach 108(2):269–274. https://doi.org/10.1115/1.3262047
22. Spurr A (1980) A computational and experimental study of fully three dimensional transonic flow in turbomachinery. Dissertation, University of Southampton
23. Squire LC (1986) Effects of probe supports on measurements in steam turbines. In: Proceedings of the ASME 1986 international gas turbine conference and exhibit. Vol 1: turbomachinery, Dusseldorf, 8-12 June, 1986. https://doi.org/10.1115/86-GT-213
24. Povey T, Jones TV, Oldfield MLG (2007) On a novel annular sector cascade technique. J Turbomach 129(1):175–183. https://doi.org/10.1115/1.2372766
25. Donovan WH (1995) Experimental and computational investigation of flow through an annular turbine cascade. Dissertation, Naval Postgraduate School
26. Hodson HP, Dominy RG (1993) Annular cascades. In: Hirsch C (ed) Advanced methods for cascade testing. NATO Research and Technology Organisation, Paris

Lapuzin *et al. Advances in Aerodynamics*   *(2024) 6:11*

Page 22 of 22

27. Lim C, Lapuzin A, Subotovich V et al (2004) Adjustable radial diffuser for the investigation of annular cascades of turbomachines. NTU KhPI Bull Power Heat Eng Process Equip
28. Lim C (2012) A method for the prediction of turbine performance characteristics through the experimental simulation of gasdynamic processes. Dissertation, National Technical University "Kharkiv Polytechnic Institute"
29. Abramovich G (1991) Applied gas dynamics. Nauka, Moscow
30. Subotovich VP, Yudin YA, Yudin AY et al (2016) On the data of aerodynamic computations of axiannular divergent cones. NTU KhPI Bull Power Heat Eng Process Equip 10(1182):131–135. https://doi.org/10.20998/2078-774x.2016.10.19

Publisher's Note

Springer Nature remains neutral with regard to jurisdictional claims in published maps and institutional affiliations.